# Application of an adaptive tuned vibration absorber on a dual lay-shaft dual clutch transmission powertrain for vibration reduction

Pu Gao[a,b], Paul D. Walker[b], Hui Liu[a*], Shilei Zhou[b], Changle Xiang[a]

[a] School of Mechanical Engineering, Beijing Institute of Technology, Beijing, China;

[b] School of Electrical, Mechanical and Mechatronic Systems, University of Technology Sydney, Sydney, Australia;

**Abstract**

This paper investigates the application of adaptive tuned vibration absorbers (ATVAs) to lightly damped automotive powertrains. In achieving this, it performs vibration characteristic analysis of a dual lay-shaft dual clutch transmission (DCT) equipped powertrain system, including natural frequency evaluation and sensitivity studies. These are coupled with the evaluation of transient response due to gear change and the variation of both gear ratio and engine speed. Results demonstrate that the impact of ATVAs on transient response during gear change is minimal, suggesting these short duration transients are outside the scope of application for ATVAs. However as excitation forces originate from the engine, its speed has a significant impact on excitation frequency. Furthermore, the gear ratios significantly influence engine operating range and natural frequency in any particular gear. Therefore, variation of engine speeds and gear ratios are the main influencing factors affecting the dominant excitation frequency. Consequently, the relationships among the system natural frequencies, the dominant external excitation frequency and the inherent frequency of the ATVA are comprehensively studied. by investigating the relationship between the dominant external excitation frequency and system natural frequencies and the system sensitivity analysis results, the installation position, stiffness range and optimal frequency tuning scheme of the ATVA can be determined. Results were applied to a DCT powertrain in 2$^{nd}$ gear and 4$^{th}$ gear with continuously changing engine speeds, an ATVA with corresponding variable stiffness and frequency tuning scheme is installed on the powertrain for vibration reduction. By comparing the simulation results, the effectiveness and reliability of the ATVA installation position, the stiffness range and the optimal frequency tuning scheme proposed in this study can be verified.

**Keywords:** adaptive tuned vibration absorbers; automotive powertrains; dominant external excitation frequency; system natural frequencies; inherent frequency of the ATVA; installation position; optimal frequency tuning scheme

## 1. Introduction

With the increasing power density of vehicular driveline technologies, various high-performance power conversion systems have been introduced. The dual clutch transmission (DCT) powertrain is one of the most widely adopted structures in the current market. It uses traditional gears and synchronizers combined with precise clutch control to realize automatic, high-efficiency driving performance. Accurate coordinated control of the hydraulic system, synchronizers and clutch are required in the DCT powertrain [1-3]. Kulkarni et al. [4] performed a detailed study of DCT powertrain control. The DCT powertrain includes the engine, DCT, gearbox, synchronizers, differential and wheels. Because of its many components and state dependent configurations, this type of powertrain is a wideband vibration system with multiple natural frequencies [5-7]. Whilst operating under complex conditions, the varying external excitation can excite natural vibrations across multiple orders, resulting in vibration-induced deterioration of the system. Crowther et al. [8] analyzed the NVH characteristics of a planetary automatic transmission equipped powertrain and provided typical examples of such behavior. Lumped mass models are widely used to accurately describe dynamic systems and study their dynamic characteristics [9], and this method is adopted in the present study.

In DCT powertrains, the odd gear shaft and even gear shaft are driven by two separate clutches, this enabling power-on gear shifting processes. However, when the engine output torque changes under stable driving conditions, the powertrain torsional vibrations remain substantial and affect the whole system. Well-designed and properly installed dynamic vibration absorbers can effectively improve the dynamic characteristics of the system and reduce system vibration. Dynamic vibration absorbers are classified as passive dynamic absorbers, active dynamic absorbers and semi-active dynamic absorbers or adaptive tuned vibration absorbers (ATVAs). Semi-active dynamic absorbers with tunable parameters are widely used. A semi-active dynamic absorber can change the system inherent frequency to track external excitation frequency, leading to its own resonance, reducing the vibration of the primary system. Semi-active dynamic absorbers can be classified as damping-tunable and frequency-tunable absorbers. Frequency-tunable absorbers are further classified as mass-tunable and stiffness-tunable absorbers; stiffness-tunable semi-active vibration absorbers are used more frequently due to their simple structure and ease of controllability [10-11].

The development of smart materials has accelerated the improvement of semi-active dynamic vibration absorbers. Williams applied a shape memory alloy to dynamic vibration absorbers. The stiffness of the shape memory alloy changes with temperature, and thus the natural frequency of the dynamic vibration absorber is adjusted to absorb system vibration [12]. Davisa adopted piezoelectric ceramics as the core part of a stiffness-tunable vibration absorber. The stiffness of piezoelectric ceramics can be controlled by an electric field to attain different absorber frequencies [13].

Magneto-rheological technology has also attracted increasing attention in recent years. The adjustable stiffness characteristics of magnetorheological elastomers is transferred to the adjustable frequency characteristic of the vibration absorbers. Various magnetorheological dynamic vibration absorbers have been designed, and notable vibration absorption characteristics have been achieved in tests [14-17]. Hoang et al. [18] designed a torsional vibration absorber with a magnetorheological elastomer to reduce powertrain vibration. Gao et al. [19] installed an ATVA group on the vehicle powertrain and studied the changes in dynamic characteristics. In addition, parameter optimization and coordinated control were conducted to achieve the optimal vibration reduction.

Vehicles drive under a wide range of operating conditions. During gear shifting and engine acceleration, resonance in the powertrain is more severe, leading to the deterioration of the vehicle's NVH characteristics. In previous research, vibration absorbers have been installed in powertrains with no clear application scope. This paper defines the effective application scope of the ATVA by analyzing the effects of engine speed variation, gear ratio variation and the gear shifting processes on the dominant external excitation frequency. Moreover, the relationships among system natural frequencies, the dominant external excitation frequency and the inherent frequency of the dynamic vibration absorber are comprehensively studied. Based on the relationship between the dominant external excitation frequency and system natural frequencies and the results of the system sensitivity analysis, the installation position and stiffness range of the vibration absorbers can be determined. In addition, based on the relationship between the dominant external excitation frequency and inherent dynamic vibration absorber frequency, the optimal frequency tuning scheme of the ATVA for preventing the coupling point of the natural vibration frequencies of the powertrain from entering the resonance area of the external excitation can be

obtained. The developed analytical process can be used as a standard to provide guidance for the application of ATVA for powertrain vibration reduction.

The rest of the paper is organized as follows. In Section 2, a multi-DOF dynamic model of a dual lay-shaft DCT powertrain is established, the natural vibration analysis and system sensitivity analysis are presented. Additionally, an appropriate engine excitation model and vehicle resistance model that can be integrated into the system dynamic model are built. In Section 3, the main factors affecting the dominant external excitation frequency are analyzed, including the gear shifting transient process, engine speed variation and gear ratios. The effective application scopes of ATVAs can thus be determined. In Section 4, the relationships among the system natural frequencies, dominant external excitation frequency and inherent frequency of the ATVA are comprehensively studied. Based on the relationship between the dominant external excitation frequency and system natural frequencies and the results of the system sensitivity analysis, the installation position and stiffness range of the ATVA can be determined. Based on the relationship between the dominant external excitation frequency and the inherent ATVA frequency, the optimal frequency tuning scheme of the ATVA is obtained. In Section 5, the ATVA is applied to the DCT powertrain when the system is in $2^{nd}$ gear and in $4^{th}$ gear as examples to demonstrate the importance of analyzing the overall relationship among the dominant external excitation frequency, system natural frequencies and inherent frequency of the dynamic vibration absorber. The conclusions and highlights are given in Section 6.

## 2. Vibration characteristics analysis of the dual lay-shaft DCT powertrain

### *2.1 Natural vibration characteristics analysis of the dual lay-shaft DCT powertrain*

The dual lay-shaft DCT powertrain is idealized as a 6 degrees of freedom torsional vibration system [20]. The advantage of the dual lay-shaft DCT versus the single lay-shaft DCT is that the synchronizers do not lie on the power-transmitting route; thus, the dual lay-shaft DCT can be used as a moving inertia vibration absorber to partially absorb the system vibrations. A schematic diagram is shown in Fig. 1.

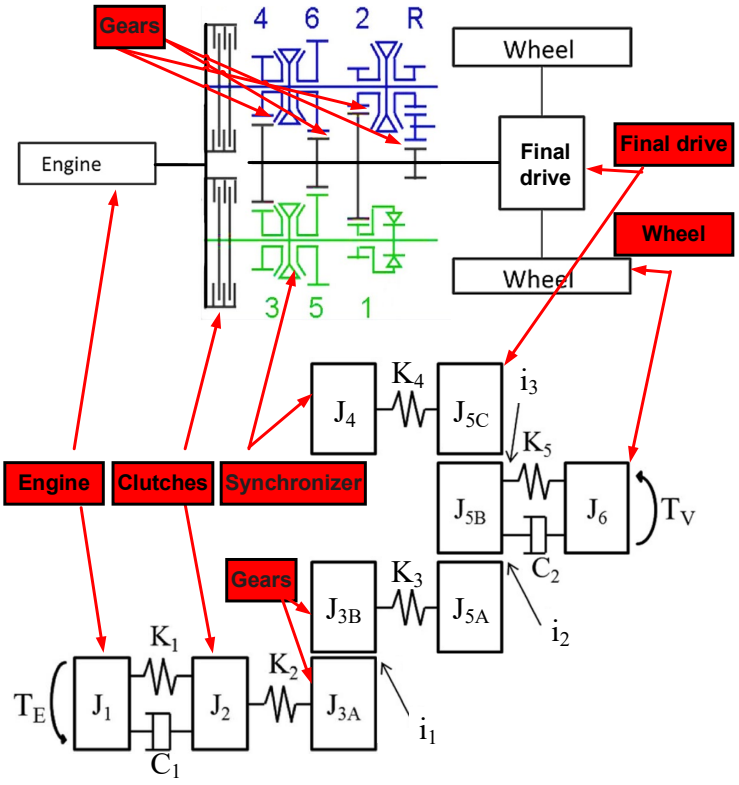


Fig. 1 Schematic diagram of the powertrain

The dynamic equations are as follows:

$$\begin{cases} J_1\ddot{\theta}_1 - C_1(\dot{\theta}_2 - \dot{\theta}_1) - K_1(\theta_2 - \theta_1) = T_E \\ J_2\ddot{\theta}_2 + C_1(\dot{\theta}_2 - \dot{\theta}_1) + K_1(\theta_2 - \theta_1) - K_2(i_1\theta_{3B} - \theta_2) = 0 \\ (J_{3B} + i_1^2 J_{3A})\ddot{\theta}_{3B} + i_1 K_2(i_1\theta_{3B} - \theta_2) - K_3(i_2\theta_{5B} - \theta_{3B}) = 0 \\ J_4\ddot{\theta}_4 - K_4(i_3\theta_{5B} - \theta_4) = 0 \\ (J_{5B} + i_2^2 J_{5A} + i_3^2 J_{5C})\ddot{\theta}_{5B} + i_2 K_3(i_2\theta_{5B} - \theta_{3B}) + i_3 K_4(i_3\theta_{5B} - \theta_4) - K_5(\theta_6 - \theta_{5B}) - C_2(\dot{\theta}_6 - \dot{\theta}_{5B}) = 0 \\ J_6\ddot{\theta}_6 + K_5(\theta_6 - \theta_{5B}) + C_2(\dot{\theta}_6 - \dot{\theta}_{5B}) = -T_V \end{cases} \quad (1)$$

where $J_1$ is the inertia of the engine; $J_2$ is the inertia of the flywheel and clutch; $J_3$ is the inertia of the gear pairs; $J_4$ is the inertia of the synchronizers; $J_5$ is the inertia of the differential; $J_6$ is the inertia of the wheel.

Eq. (1) can be expressed as：

$$J\ddot{\theta} + C\dot{\theta} + K\theta = T \quad (2)$$

Where $\theta$ indicates the angle displacements of every inertial element, $\theta = [\theta_1 \quad \theta_2 \quad \theta_{3B} \quad \theta_4 \quad \theta_{5B} \quad \theta_6]$, and $T$ indicates the external excitation, $T = [T_E \quad 0 \quad 0 \quad 0 \quad 0 \quad -T_V]$. The system mass matrix, damping matrix and stiffness matrix are as follows:

$$J=\begin{bmatrix} J_1 & 0 & 0 & 0 & 0 & 0 \\ 0 & J_2 & 0 & 0 & 0 & 0 \\ 0 & 0 & J_{3B}+i_1^2 J_{3A} & 0 & 0 & 0 \\ 0 & 0 & 0 & J_4 & 0 & 0 \\ 0 & 0 & 0 & 0 & J_{5B}+i_2^2 J_{5A}+i_3^2 J_{5C} & 0 \\ 0 & 0 & 0 & 0 & 0 & J_6 \end{bmatrix} \quad (3)$$

$$C=\begin{bmatrix} C_1 & -C_1 & 0 & 0 & 0 & 0 \\ -C_1 & C_1 & 0 & 0 & 0 & 0 \\ 0 & 0 & 0 & 0 & 0 & 0 \\ 0 & 0 & 0 & 0 & 0 & 0 \\ 0 & 0 & 0 & 0 & C_2 & -C_2 \\ 0 & 0 & 0 & 0 & -C_2 & C_2 \end{bmatrix} \quad (4)$$

$$K=\begin{bmatrix} K_1 & -K_1 & 0 & 0 & 0 & 0 \\ -K_1 & K_1+K_2 & -i_1K_2 & 0 & 0 & 0 \\ 0 & -i_1K_2 & i_1^2K_2+K_3 & 0 & -i_2K_3 & 0 \\ 0 & 0 & 0 & K_4 & -i_3K_4 & 0 \\ 0 & 0 & -i_2K_3 & -i_3K_4 & i_2^2K_3+i_3^2K_4+K_5 & -K_5 \\ 0 & 0 & 0 & 0 & -K_5 & K_5 \end{bmatrix} \quad (5)$$

The damped free-vibration system is transferred into state space with initial values:

$$\begin{cases} A\dot{v}(t)+Bv(t)=0 \\ v(0)=v_0 \end{cases} \quad (6)$$

Where $A=\begin{bmatrix} C & J \\ J & 0 \end{bmatrix}$, $B=\begin{bmatrix} K & 0 \\ 0 & -J \end{bmatrix}$, $v(t)$ is the generalized vector $v(t)=\psi q(t)$, $\psi$ is the complex eigenvector $\psi=[\tilde{\psi} \quad \tilde{\psi}\lambda]^T$, $\lambda$ is the complex eigenvalue $\lambda_r=h_r\pm i\omega_r$, $\omega_r$ is the system $r^{th}$ natural angle frequency, and $\zeta_r$ is the damping ratio $\zeta_r=\frac{-h_r}{\omega_r}$.

Therefore, we obtain the following equation:

$$(A\lambda+B)\begin{Bmatrix} \tilde{\psi} \\ \tilde{\psi}\lambda \end{Bmatrix}=0 \quad (7)$$

The eigenvalue $\lambda$ and eigenvector $\psi$ are obtained via complex eigenvalue analysis. The natural frequencies, corresponding modal shapes and damping ratio can then be obtained.

The system parameters are shown in Table 1.

Table 1 System parameters

| Inertia（kg·m$^2$） | | Stiffness（N·m·rad$^{-1}$） | Damping（N·m·s·rad$^{-1}$） |
|---|---|---|---|
| Engine | $J_1=0.40$ | $K_1=10000$ | $C_1=20$ |
| Flywheel and clutch | $J_2=0.40$ | $K_2=20000$ | $C_2=50$ |
| Gears | $J_{3A}=0.0145$ $J_{3B}=0.0075$ | $K_3=100000$ | |
| Synchronizers | $J_4=0.01$ | $K_4=100000$ | |
| Differential | $J_{5A}=0.03$ $J_{5B}=1.2$ $J_{5C}=0.01$ | $K_5=2000$ | |
| Wheel | $J_6=100$ | | |

With these system parameters, the natural frequencies and damping ratio are determined, as shown in Table 2.

Table 2 Natural frequencies and related damping ratios

| Order | Frequency (Hz) | Damping ratio (%) |
|---|---|---|
| 1 | 0.00 | -- |
| 2 | 1.60 | 12.50 |
| 3 | 33.21 | 22.03 |
| 4 | 84.20 | 3.12 |
| 5 | 356.81 | 0.12 |
| 6 | 522.57 | 0.00 |

The corresponding modal shapes are shown in Fig. 2.

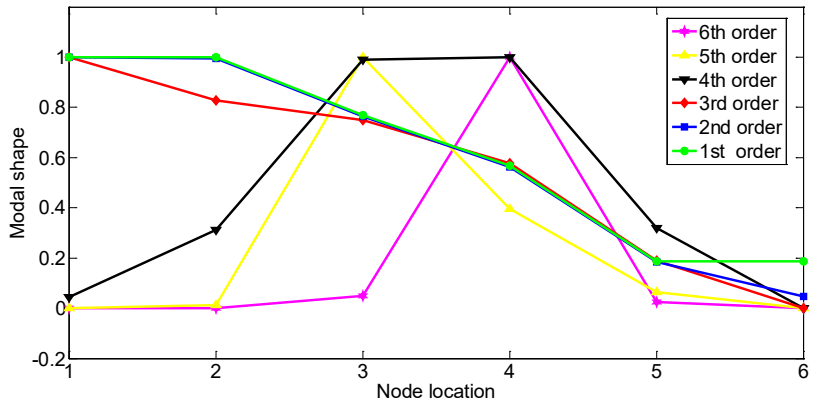


Fig. 2 Corresponding modal shapes

*2.2 Sensitivity of the eigenvalues of each order to each inertial value*

$J_n(n=1,2,3,4,5,6)$ are set as the inertial values and can be used to denote the independent variable of each sensitivity. Substituting the $r^{th}$ eigenvalue and eigenvector into Eq. (7), multiplying the left side by $\psi_r^T$ and taking the derivative of the equation [21-23], we obtain the following:

$$\frac{\partial(\psi_r^T(A\lambda_r+B)\psi_r)}{\partial J_n}=0 \tag{8}$$

$$\frac{\partial\lambda_r}{\partial J_n}=\frac{\partial\left((-A_r^{-1})B_r\right)}{\partial J_n} \tag{9}$$

$$\frac{\partial\lambda_r}{\partial J_n}=\frac{\partial(-A_r^{-1})}{\partial J_n}B_r+(-A^{-1})\frac{\partial B_r}{\partial J_n} \tag{10}$$

$$\frac{\partial \lambda_r}{\partial J_n} = \frac{\psi_r^T \partial(-A^{-1})\psi_r}{\partial J_n} \psi_r^T B \psi_r + \psi_r^T (-A^{-1}) \psi_r \frac{\psi_r^T \partial B \psi_r}{\partial J_n} \qquad (11)$$

Where

$$A = \begin{bmatrix} C & J \\ J & 0 \end{bmatrix} \quad B = \begin{bmatrix} K & 0 \\ 0 & -J \end{bmatrix} \qquad (12)$$

Substituting the relevant sub modules $\frac{\partial(-A^{-1})}{\partial J_n}$ and $\frac{\partial B}{\partial J_n}$ into the above equation, we can obtain the sensitivities of the eigenvalues of each order to each inertial value. The results are shown in Fig. 3 – Fig. 8.

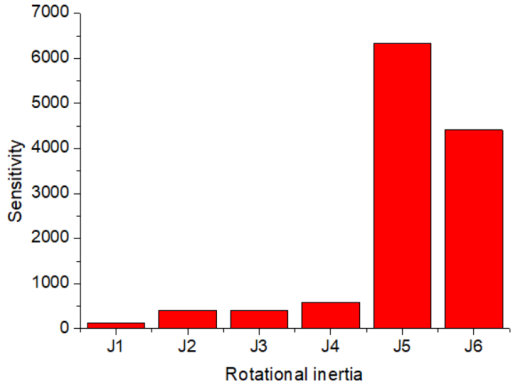


Fig. 3 Sensitivity of the $1^{st}$ -order eigenvalue

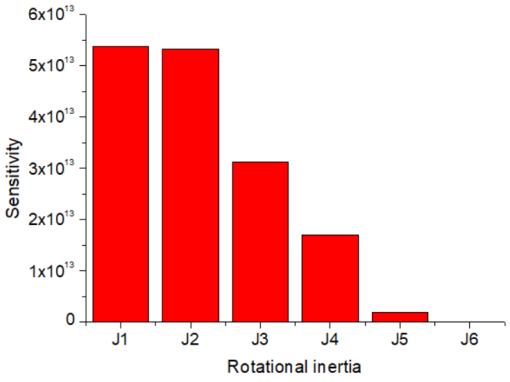


Fig. 4 Sensitivity of the $2^{nd}$ -order eigenvalue

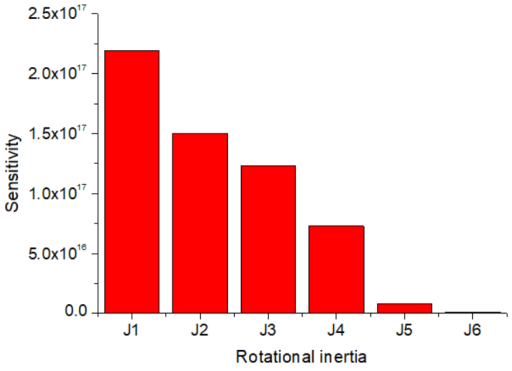


Fig. 5 Sensitivity of the $3^{rd}$ -order eigenvalue

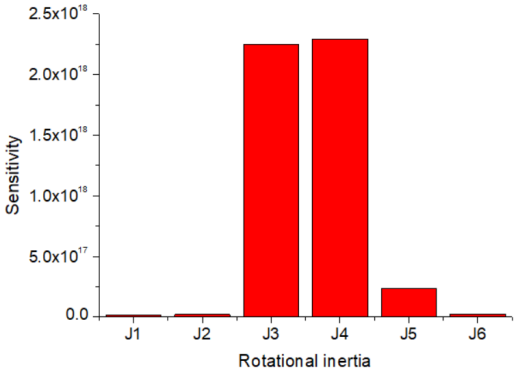


Fig. 6 Sensitivity of the $4^{th}$ -order eigenvalue

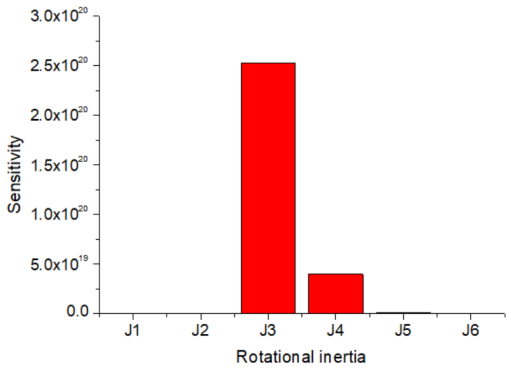


Fig. 7 Sensitivity of the $5^{th}$ -order eigenvalue

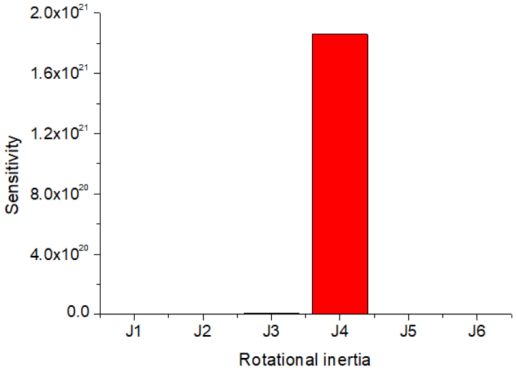


Fig. 8 Sensitivity of the $6^{th}$ -order eigenvalue

As shown in Fig. 3 – Fig. 8, the $1^{st}$-order natural vibration is affected mainly by inertia $J_5$, the $2^{nd}$-order natural vibration is relatively sensitive to inertias $J_1$ and $J_2$, the $3^{rd}$-order natural vibration is affected mainly by inertia $J_1$, the $4^{th}$-order natural vibration is affected mainly by inertias $J_4$ and $J_3$, the $5^{th}$-order natural vibration is affected mainly by inertia $J_3$, and the $6^{th}$-order vibration is sensitive primarily to inertia $J_4$. The same conclusion can be obtained from the modal shapes in Fig. 2.

### *2.3 Engine excitation model and vehicle resistance model*

#### *2.3.1 Engine excitation model*

Various methods have been proposed for engine output torque modelling. The empirical method and look-up table method cannot describe the engine transient torque and thus cannot be used to characterize the engine harmonic excitation on the powertrain with the ATVA [4, 24]. Taylor [25] built an engine model considering the engine ignition excitation and piston rod reciprocating motion inertia. Other models use the sine wave to describe the harmonic vibration caused by ignition [8, 9, 26]. These models can be used to analyze the changeable torque responses. In this study, the effect of varying the engine speed on the harmonic excitation is described by the following equation:

$$T_E = T_{E0} + A_1 T_{E0} \sin\left(n_1 \dot{\theta}_1 t\right) + A_2 T_{E0} \sin\left(n_2 \dot{\theta}_1 t\right) + \cdots \qquad (13)$$

$T_{E0}$ is the average torque, i.e., 100 Nm. $A_1$ and $A_2$ are the amplitudes and are set to 1.8 and 0.7, respectively, for an inline 4 cylinder engine. $n_1$ and $n_2$ are the dominant harmonics and are set to 2 and 4, respectively, for an inline 4 cylinder engine. $\dot{\theta}_1$ is the engine speed, 100 rad/s. The instantaneous engine torque as a percent of the mean torque is shown in Fig. 9.

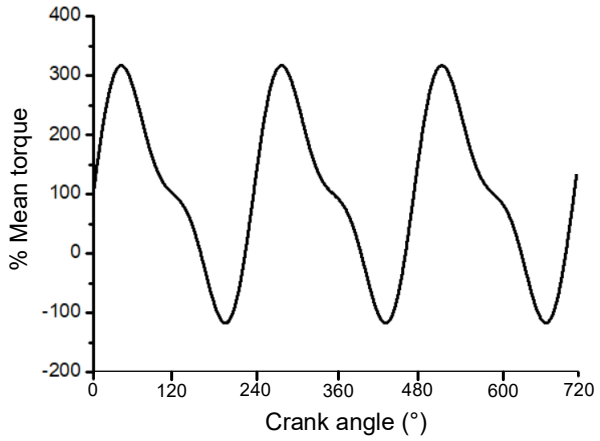

Fig. 9 Instantaneous engine torque as a percent of the mean torque

*2.3.2 Vehicle resistance model*

The engine output torque includes the mean output torque and fluctuation torque. To study the effect of the fluctuation torque on the powertrain system, the vehicle resistance is considered to balance the mean output torque, which is significant to guarantee the accuracy of the simulation. Vehicle resistance consists mainly of rolling resistance, air resistance and gradient resistance [26-28], as shown in Eq. (14):

$$T_V = \left(C_R m_V g \cos\phi + m_V g \sin\phi + 0.5 C_D \rho A_V \theta_6^2 r_T^2\right) \times r_T \qquad (14)$$

The parameters related to the vehicle resistance are shown in Table 3.

Table 3 Parameters related to the vehicle resistance

| Name | Symbol | Value |
|---|---|---|
| Rolling coefficient | $C_R$ | 0.018 |
| Vehicle mass | $m_V$ | 1780 |
| Gravitational acceleration | $g$ | 9.800 |
| Angle of slope | $\phi$ | 0.000 |
| Air coefficient | $C_D$ | 0.300 |
| Air density | $\rho$ | 1.290 |
| Frontal area | $A_V$ | 2.530 |
| Rolling angle | $\theta_6$ | -- |
| Rolling radius | $r_T$ | 0.317 |

Based on Eq. (14) and the parameters in Table 3, we can obtain the relative real vehicle resistance.

The above appropriate engine excitation model and vehicle resistance model can be integrated into the dynamic model of the DCT powertrain to establish its excitation

and constraint conditions.

## 3. Influencing factors affecting the dominant external excitation frequency

According to vibration absorption theory, adding one or more variable-stiffness magnetorheological vibration absorbers to the powertrain can reduce its driveline vibration. In the vibration absorber control, the dominant external excitation frequency (followed by the natural frequency of the ATVA) is the key item. Studying the main factors causing the excitation dominant frequency change is important and can facilitate the investigation of the effective application scope of the ATVA.

Under stable work conditions, the powertrain vibration response depends on the powertrain itself, including the engine speed, gearbox ratio and transient gear shifting process. In this section, the effect of these factors on the dominant external excitation frequency is studied in detail.

### *3.1 Influence of the gear shifting process on the torque excitation dominant frequency*

Based on the dual lay-shaft DCT powertrain model in Section 2, the engine excitation parameters can be set as follows: $T_{E0}$ is 100 Nm; $A_1$ and $A_2$ are 1.8 and 0.7, respectively; $n_1$ and $n_2$ are 2 and 4, respectively; and $\dot{\theta}_1$ is 100 rad/s.

The dual clutch is used to control the gear shifting process to change from 1st gear to 6th gear, and the dynamic response signals of the powertrain system can be collected by an oscilloscope. The control pressure of the dual clutch is shown in Fig. 10. The 1st, 3rd and 5th gears are controlled by clutch 1, and the 2nd, 4th and 6th gears are controlled by clutch 2. In the powertrain model, the transient gear shifting process can be realized by changing the clutch pressure.

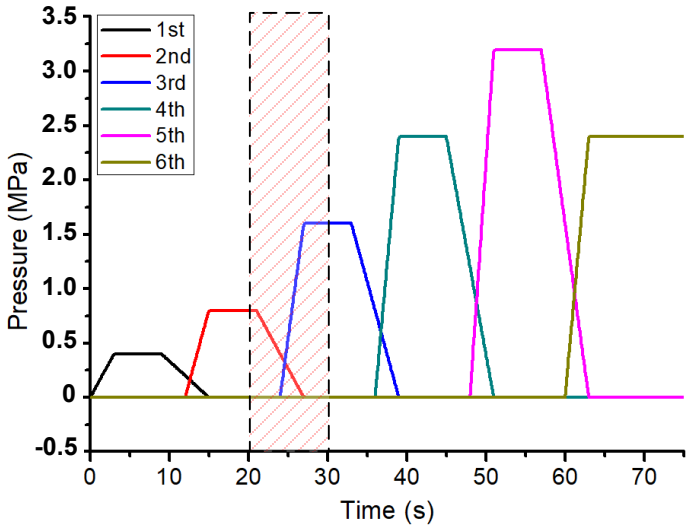

Fig. 10 Clutch pressure signal

During the gear shifting process, an oscilloscope is mounted between J1 and J2 to record the relative acceleration response of the two inertial elements, and the results are shown in Fig. 11.

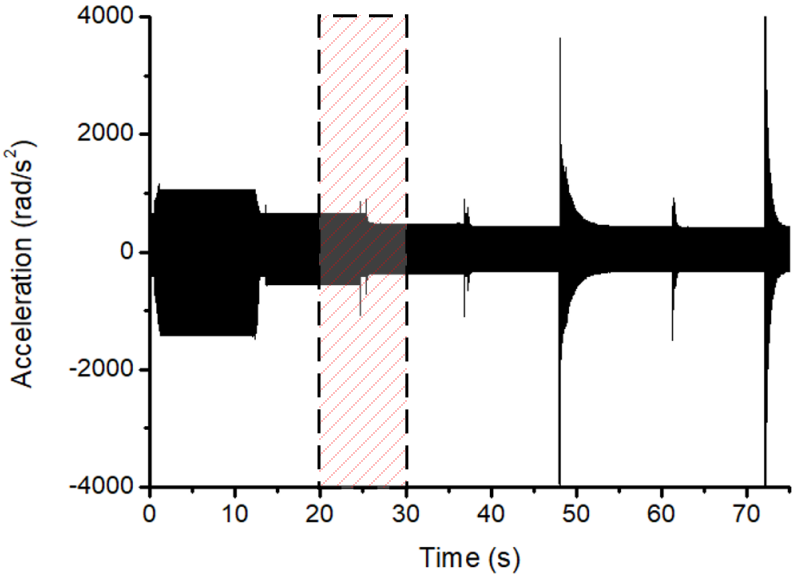

Fig. 11 $\theta_2$-$\theta_1$ acceleration response in the time domain

The acceleration response in the time domain poorly describes the system's dynamic characteristics, and thus, transformation to the frequency domain is required. The relative displacement response between the two inertia values is an unstable signal that cannot be analyzed by the fast Fourier transform (FFT); however, the Hilbert-Huang transform (HHT) [29-31] can be used to study the time signal by

processing the signal via empirical mode decomposition (EMD), transforming the unstable signal into multiple stationary signals. The HHT is then used for energy demodulation to convert the time-domain information into three-dimensional information regarding time, frequency and vibration energy for comprehensive analysis. The effect of the transient gear shifting process on the dominant external excitation frequency is the research goal in this section. The process of shifting gears from 2nd gear to 3rd gear is selected for comprehensive analysis. The result is shown in Fig. 12.

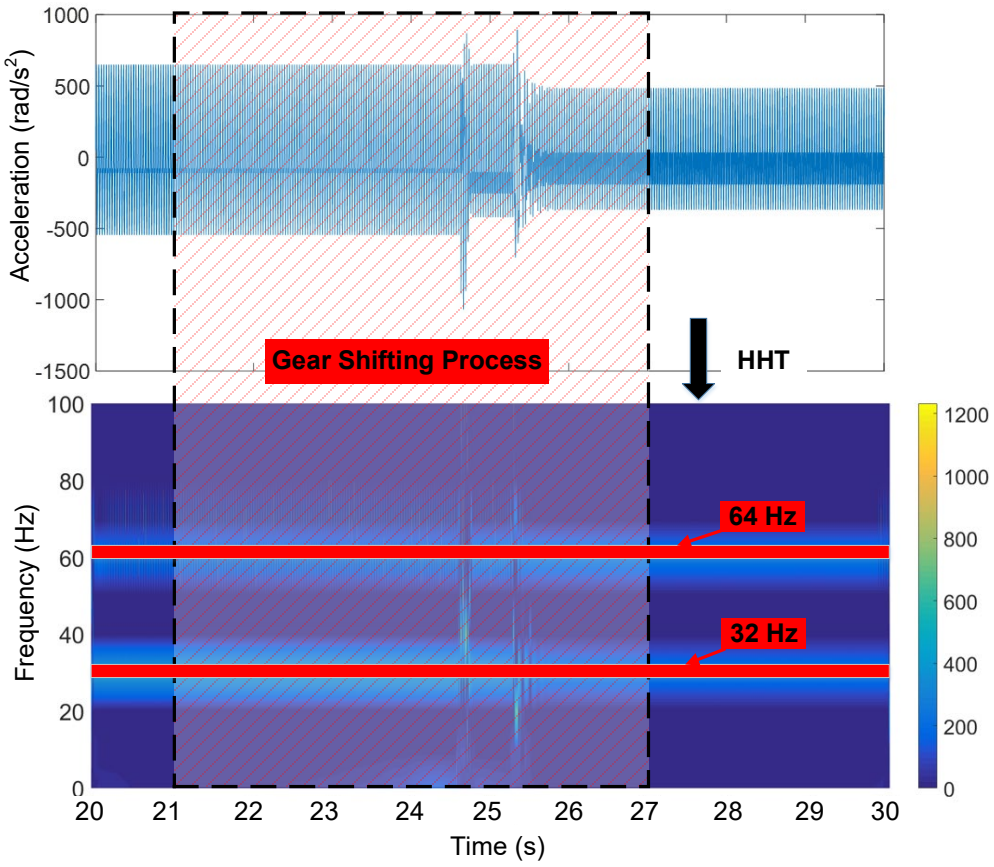


Fig. 12 Trend of the dominant external excitation frequency obtained by the HHT

The process of shifting gears begins at 21 s and ends at 27 s. During this period, the signal dominant frequencies are the dominant rotation frequencies of the engine, which are 32 Hz and 64 Hz, corresponding to the strong and main harmonics 2 and 4 of the inline 4-cylinder engine, respectively. The signal dominant frequency changes suddenly at 24.5 s and 25.5 s, which has little effect on the dominant excitation frequency during the whole gear shifting process. Gear shifting is a transient process with a short duration that has little effect on the overall stable acceleration signal. The

process of engaging the clutch can significantly affect the powertrain, but this impact would be reflected in the vibration magnitude and not the vibration frequency.

The fundamental principle that defines the application of vibration absorbers is that it follows the dominant external excitation frequency. The gear shifting process has little impact on the dominant external excitation frequency and acts only briefly, and the vibration absorber has a limited ability to change characteristics instantly. Although the vibration magnitude is reduced in this process with the vibration absorber, the reduction of the magnitude is a damping effect and is outside the effective application scope of the ATVA. The vibration problem of the transient gear shifting process should be solved in another way.

### *3.2 Influence of the engine speed and gear ratio on the torque excitation dominant frequency*

Similarly, based on the dual lay-shaft DCT model, the engine excitation parameters are set as follows: $T_{E0}$ is 100 Nm; the magnitudes of $A_1$ and $A_2$ are 1.8 and 0.7, respectively; $n_1$ and $n_2$ are 2 and 4, respectively; $\dot{\theta}_1$ ranges from 1500 r/min to 4500 r/min, corresponding to 157 rad/s and 471 rad/s, respectively; the gear ratios $i_1$ from 1st gear to 6th gear are 3.46, 2.05, 1.30, 0.90, 0.91, and 0.76; the differential gear ratios $i_2$ are 4.12 and 3.04, corresponding to 1st to 4th gear and 5th to 6th gear, respectively; and the differential gear ratios $i_3$ are 3.04 and 4.12, corresponding to 1st to 4th gear and 5th to 6th gear, respectively.

To study the influence of the engine speed and gear ratio on the torque excitation dominant frequency, the engine speed changes with linear growth in different gears. The engine speed, gear ratio and differential gear ratio are shown in Fig. 13.

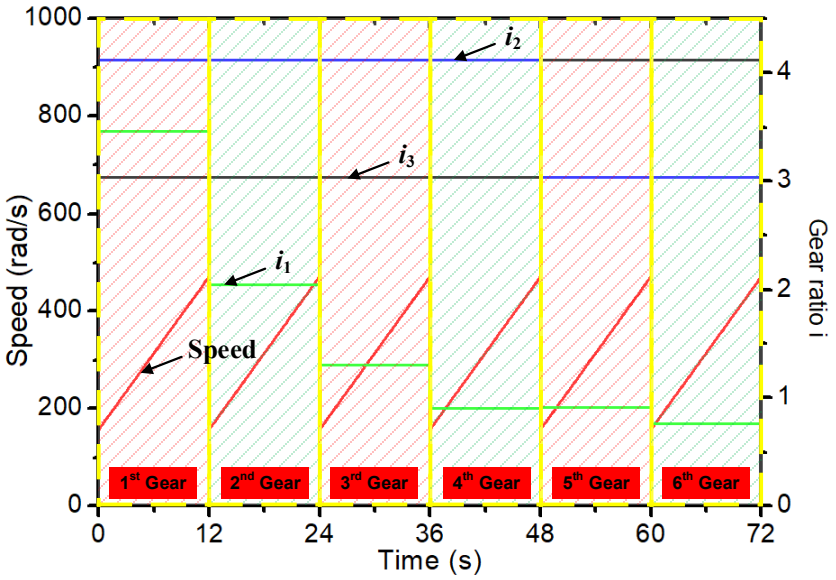


Fig. 13 Engine speed, gear ratio and differential gear ratio

The acceleration time-domain signal is studied between $J_1$ and $J_2$ to investigate the influence of the engine speed and different gear ratios on the torque excitation dominant frequency. The acceleration time-domain signal cannot describe the system dynamic characteristics, and thus, transformation to the frequency domain is required, as shown in Fig. 14.

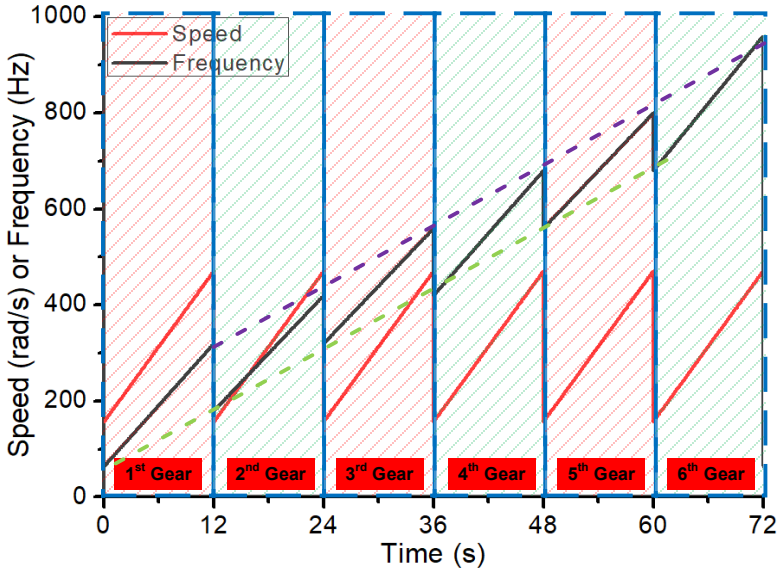


Fig. 14 Trends of the engine speed and torque excitation dominant frequency for different gear ratios

Fig. 14 illustrates that in each gear, the torque excitation dominant frequency

linearly increases with the linear increase of the engine speed. The starting and ending points are different and increase with the increment of the gear ratios. As shown in Fig. 14, the dominant torque excitation frequency is affected mainly by the engine speed and gear ratios.

The torque excitation in the powertrain is a mixture of signals with various frequencies and magnitudes. It is challenging to identify the dominant frequency of the torque excitation in real time. Thus, extracting the dominant torque excitation frequency ranges of the normal engine working speeds at each gear ratio is necessary to improve the accuracy and reliability of the complex signal frequency identification, which is beneficial for following the frequency of the ATVA. According to Fig. 14, the frequency ranges of the torque excitation for the engine working at different gear ratios can be attained, as shown in Table 4.

Table 4 Dominant excitation frequency ranges at the normal engine working speeds in different gears

| Gear | Frequency (Hz) |
|---|---|
| 1st | 64-320 |
| 2nd | 180-420 |
| 3rd | 320-560 |
| 4th | 420-680 |
| 5th | 560-800 |
| 6th | 680-960 |

As shown in Table 4, the gear ratios can be used to divide the dominant frequency of the torque excitation into different segments, which is beneficial for the real-time signal frequency identification of the complex torque excitation and for improving the calculation efficiency.

## 4. Relationships among the system natural frequencies, dominant external excitation frequency and inherent frequency of the ATVA

The ATVA can be used to reduce the powertrain vibration, and the relationships among the system natural frequencies, dominant external excitation frequency and inherent frequency of the ATVA should be studied in detail and optimally matched. The ATVA with the best vibration reduction performance should be mounted in a proper position to achieve the optimal vibration reduction effect.

The system natural frequencies reflect the vibration characteristics of the powertrain system and depend on the powertrain system itself. The natural vibration characteristics cannot change under different external excitations, and thus the torque excitation frequency and system natural frequencies appear to be independent. However, if these two frequencies are near each other, resonance occurs. In addition, the system natural frequencies will change with ATVA installation on the powertrain.

The dominant frequency of torque excitation is determined by engine speed and gear ratios. Transient processes, such as the gear shifting process, have little impact on the dominant excitation frequency. Resonance occurs if the torque excitation frequency approaches the system natural frequencies, thus degrading the system NVH characteristics. When the torque excitation frequency approaches the ATVA natural frequency, resonance occurs in the vibration absorber, and the vibration energy is absorbed by the ATVA, thereby improving the system NVH characteristics. The torque excitation frequency is the main factor in the relationships among the three frequencies.

The inherent frequency of the ATVA reflects the absorber's vibration characteristics and depends on the vibration absorber mass and changeable stiffness elastomer. The ATVA's natural frequency can be tuned as the torque excitation frequency changes. Resonance occurs on the moving mass, and the powertrain vibration energy can be absorbed from the driveline. The ATVA is semi-active, and thus the vibration absorber natural frequency is the only controllable factor in the relationships among the three frequencies. The relationships of the three frequencies can be optimized by controlling the inherent frequency of the ATVA to achieve the best vibration reduction effect.

### *4.1 Relationship between the dominant external excitation frequency and system natural frequencies*

Resonance occurs in the powertrain system when the dominant excitation frequency approaches the system natural frequencies. The dominant torque excitation frequency is determined mainly by the engine speed and gear ratios. The system natural frequencies reflect only the system’s dynamic characteristics and depend on the powertrain system itself. At different gear ratios, the torque excitation dominant frequency linearly increases with the linear increase of the engine speed and is compared with the system natural frequencies in Fig. 15.

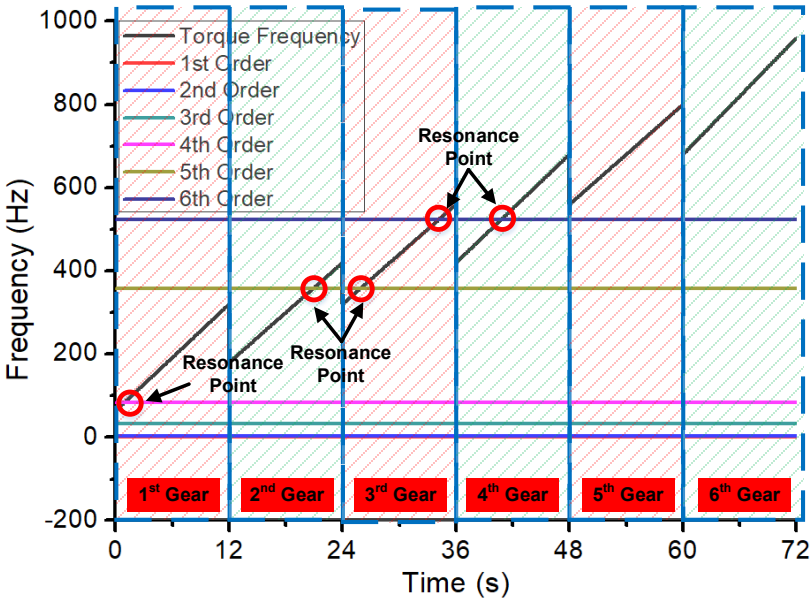


Fig. 15 Relationship between the excitation dominant frequency and system natural frequencies

At different gear ratios, the powertrain system frequencies are similar and are nearly constant under the entire working range.

When the powertrain system is in 1st gear, the 4th natural frequency, 84.2 Hz, passes through the torque excitation range (64-320 Hz). Resonance can occur at this intersection, which is labelled resonance point 1. When the powertrain system is in 2nd gear and 3rd gear, the 5th natural frequency, 356.8 Hz, passes through the torque excitation dominant frequencies (180-420 Hz) and (320-560 Hz), respectively. Resonance occurs at these two intersections, which are labelled resonance points 2 and 3. When the powertrain system is in 3rd gear and 4th gear, the 6th natural frequency, 522.6 Hz, passes through the torque excitation ranges (320-560 Hz) and (420-680 Hz), respectively. Resonance occurs at these two intersections, which are labelled resonance points 4 and 5.

The above analysis results and the results of the system sensitivity analysis in Section 2 can provide theoretical guidance for determining the absorber installation position and changeable stiffness range. Resonance point 1 is related to the 4th natural frequency and 1st gear. From the sensitivity analysis results, $J_3$ and $J_4$ have a strong influence on the 4th natural vibration, and the vibration absorber could be installed near these two inertial elements. The 1st gear corresponds to a torque excitation

frequency range of 64-320 Hz. The absorber stiffness range can be calculated according to this range and Eq. (15). Resonance points 2 and 3 are related to the 5th natural frequency and 2nd and 3rd gears, respectively. According to the sensitivity analysis results, $J_3$ has a strong influence on the 5th natural vibration, and the vibration absorber should be installed near this inertial element. The 2nd gear- and 3rd gear-related torque excitation frequency ranges are 180-420 Hz and 320-560 Hz, respectively. The absorber stiffness range can be calculated according to these two ranges and Eq. (15). Resonance points 4 and 5 are related to the 6th natural frequency and 3rd and 4th gears, respectively. According to the sensitivity analysis results, $J_4$ has a strong influence on the 6th natural vibration, and the vibration absorber could be installed near this inertial element. The 3rd gear- and 4th gear-related torque excitation frequency ranges are 320-560 Hz and 420-680 Hz, respectively. The absorber stiffness range can be calculated according to these two ranges and Eq. (15).

$$k_A = (2\pi \cdot \omega)^2 \cdot J_A \tag{15}$$

where $k_A$ is the changeable stiffness, $\omega$ is the natural frequency of the vibration absorber, and $J_A$ is the moving inertia of the vibration absorber.

*4.2 Relationship between the dominant external excitation frequency and inherent frequency of the dynamic vibration absorber*

According to vibration absorption theory, the ATVA natural frequency follows the external excitation frequency. The vibration absorber then generates resonance, the vibration on the main powertrain is reduced, and the NVH characteristics are improved. According to reference [19], the inherent frequency of the ATVA follows the torque excitation frequency exactly and may not be the best frequency tuning scheme. After the ATVA is installed, its variable natural frequency alters the vibration characteristics of the powertrain. Vibration coupling between the new variable natural vibration frequency and other relative constant natural system vibrations should be taken into consideration. In addition, the new variable vibration frequency may enter the resonance area of the torque excitation dominant frequency, which would degrade the NVH characteristics of the powertrain system. For example, when powertrain is in 2nd gear, the engine speed increases from 1500 r/min to 4500 r/min, and the torque excitation frequency increases from 180 Hz to 420 Hz. A vibration absorber with a 100% following frequency tuning scheme is installed on $J_1$. The powertrain model is

shown in Fig. 16. The absorber parameters are $J_A = J_1/5 = 0.08$ kg·m$^2$ and $c_A = 1.23$ N·m·s·rad$^{-1}$. The changeable stiffness $k_A$ can be calculated according to the frequency tuning scheme adopted and Eq. (15).

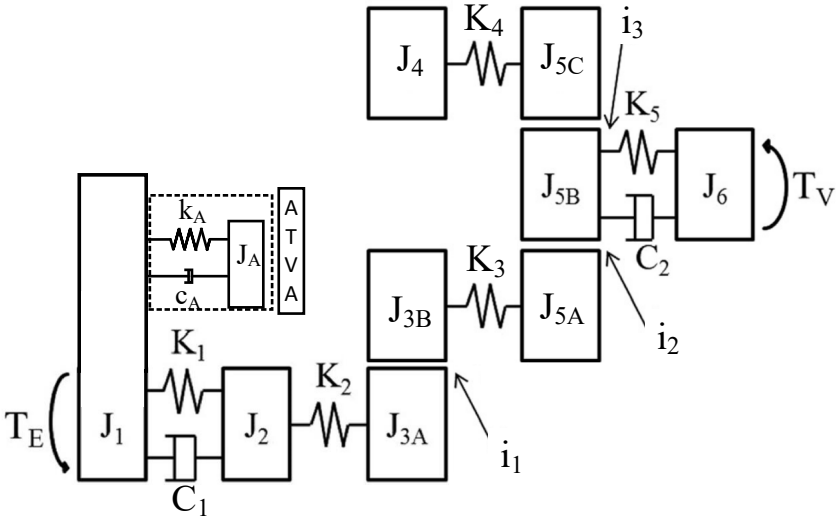


Fig. 16 Powertrain model with the vibration absorber

Between $J_1$ and $J_2$ the relative displacement time response between these two inertial values is studied. The average torque of the powertrain is filtered. The relative displacement responses without and with the vibration absorber are shown in Fig. 17.

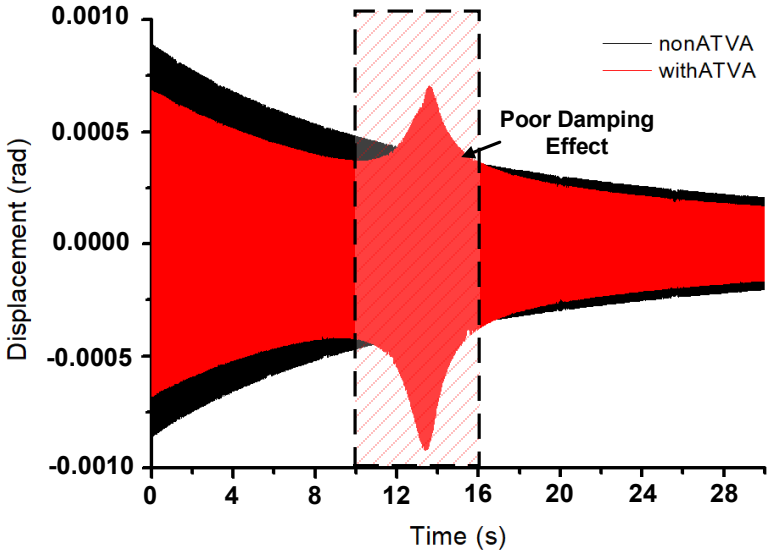


Fig. 17 $\theta_2$-$\theta_1$ displacement

The vibration response is generally improved with the ATVA, and the vibration magnitude is reduced significantly. However, in the period from 10 s to 16 s, the

vibration response deteriorates. The system natural frequencies may have changed after installing the ATVA, or one of the system natural frequencies may have entered the resonance area of the external excitation frequency. To study the reason in greater detail, the system variable natural frequencies of the powertrain with the ATVA are calculated, and the results are shown in Fig. 18.

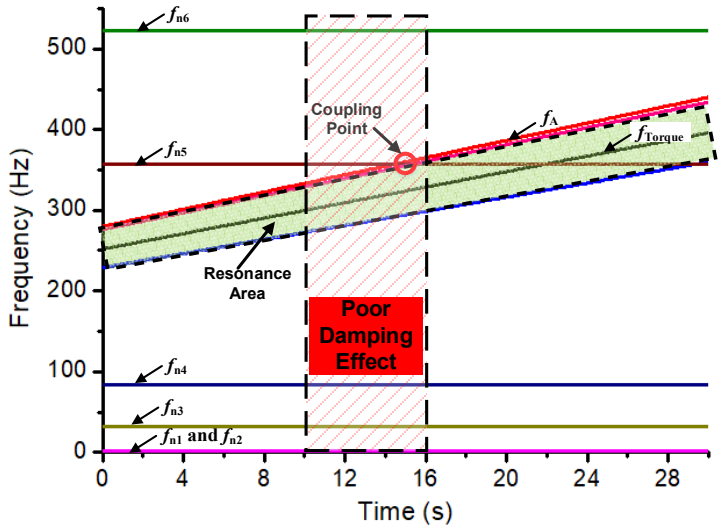


Fig. 18 System transient changeable natural vibration frequencies of the powertrain with the ATVA in 100% following frequency tuning scheme

The ATVA generates a new variable natural frequency in the powertrain $f_A$. This frequency continuously increases along the edge of the excitation resonance area. Over time, the new transient changeable natural vibration frequency passes through the 5$^{th}$ natural frequency, forming a coupling point, and these two system natural vibrations couple in this period. In addition, the coupling point is close to the resonance area of the external excitation. Therefore, the new transient changeable natural vibration frequency $f_A$ enters the excitation resonance area, and the coupling of two system natural vibrations appears in this period from 10 s to 16 s. These are the essential reasons for the vibration deterioration in Fig. 17. According to the trends of the new variable natural frequency the 6$^{th}$ natural frequency and the torque excitation frequency, the transient changeable natural vibration frequency passes through the 6$^{th}$ natural frequency, forming another coupling point. This coupling point is also close to the resonance area of the external excitation, which is expected to degrade the system vibration response.

The above analysis indicates that if the ATVA natural frequency follows the external excitation frequency with absolute fidelity, the vibration reduction effect cannot reach the optimal state, and thus the frequency tuning scheme of the ATVA should be modified. According the literature [19,32], the minimum following frequency is reduced by 30%, and the maximum frequency is increased by 30%. The system variable natural frequency of the powertrain with the modified frequency tuning scheme is shown in Fig. 19.

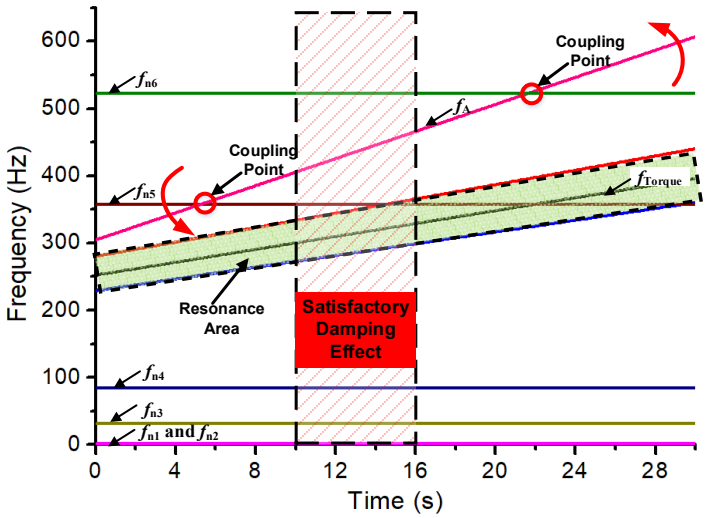


Fig. 19 System transient changeable natural vibration frequencies of the powertrain with the ATVA in modified frequency tuning scheme

After modifying the frequency tuning scheme, the natural frequency $f_A$ is still variable and can couple with the 5$^{th}$ vibration and 6$^{th}$ vibration at 6 s and 22 s, respectively, to form two coupling points. However, these two coupling points are far from the resonance area of the external excitation. Therefore, the modified frequency tuning scheme never leads to vibration deterioration at any time. To investigate this the relative vibration of $J_1$ and $J_2$ is studied. Fig. 20 shows the relative displacement responses without the ATVA, with the ATVA in the 100% frequency following scheme, and with the ATVA in the modified frequency tuning scheme.

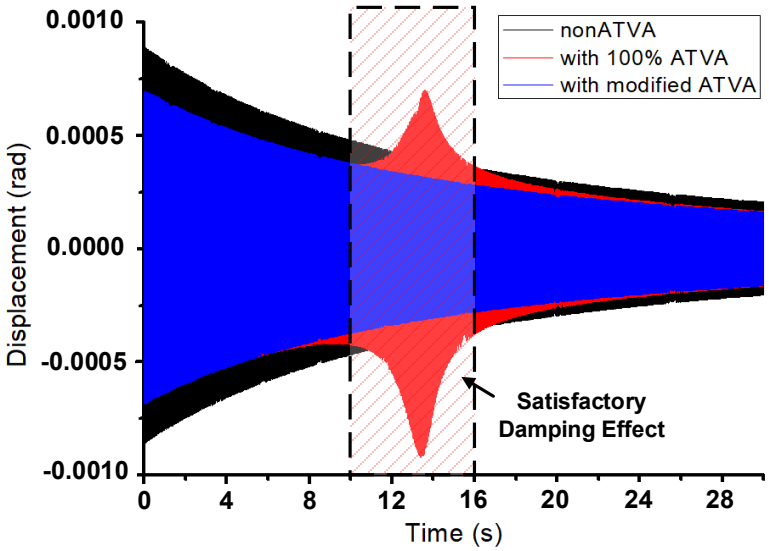


Fig. 20 Relative displacement responses of the three schemes

The improved frequency tuning scheme can prevent the coupling of the variable natural vibration frequencies entering torque excitation resonance area; thus, optimal vibration reduction effects can be attained over the entire working range.

Based on the above analysis, the best vibration reduction effect can be obtained only by considering the overall relationships of the three frequencies (system natural frequencies, dominant external excitation frequency and inherent frequency of the dynamic vibration absorber).

## 5. Application of the ATVA to the DCT powertrain

Based on the analysis of the influencing factors of the dominant external excitation frequency in Section 3, gear shifting is a transient process with a short duration and thus has little influence on the dominant frequency. The ATVA can only follow the dominant frequency and cannot effectively reduce vibration during the gear shifting process. Therefore, the transient gear shifting process is not the effective application scope of the current ATVA. As the change in the torque excitation dominant frequency depends on the engine speed and gear ratios, the ATVA can be used in the powertrain in a certain gear with continuously changing engine speed. According to the analysis results in Section 4, the ATVA is applied on the DCT powertrain for system vibration reduction.

*5.1 Application of the ATVA on the DCT powertrain in 2nd gear*

According to the analysis of the relationship between the dominant external excitation frequency and system natural frequencies in Section 4.1, when the powertrain works in 2nd gear, the 5th natural frequency, 356.8 Hz, passes through the torque excitation frequency range (180-420 Hz) to form resonance point 2. According to the sensitivity analysis result in Section 2.2, $J_3$ has a significant effect on the 5th order natural vibration; thus, the vibration absorber should be installed near $J_3$. However, $J_3$ are gear pairs in the powertrain model, and the vibration absorber cannot be easily installed at this inertial point. Instead, we install the ATVA near that inertial point, at $J_2$. The dynamic model is shown in Fig. 21.

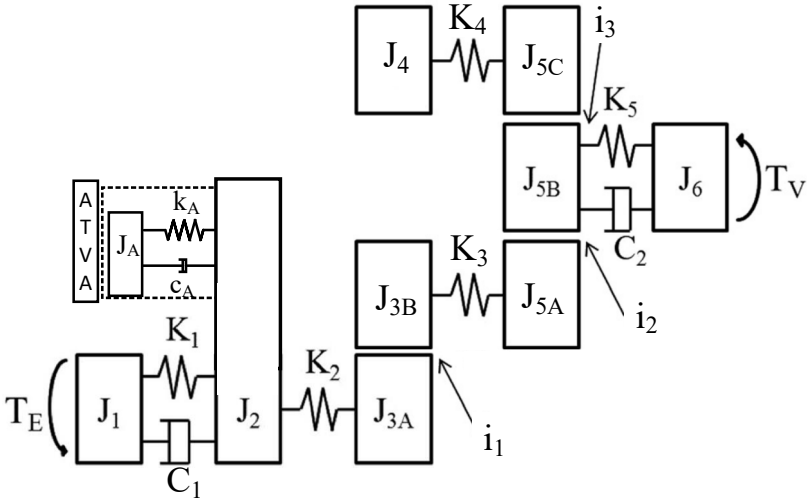


Fig. 21 Dynamic model of the powertrain with the ATVA

Two ATVA frequency tuning schemes are adopted. One is a 100% frequency following scheme; the other is the improved frequency tuning schemes described in Section 4.2. The vibration absorber parameters are as follows: moving inertia $J_A = J_2/5 = 0.08$ kg·m$^2$ and damping $c_A = 1.23$ N·m·s·rad$^{-1}$. The changeable stiffness $k_A$ can be calculated according to the frequency tuning scheme and Eq. (15).

Analysis is performed using the relative displacement time response between these two inertial elements. A comparison is made among the vibration response without the ATVA, with the ATVA in the 100% frequency following scheme, and with the ATVA in the modified frequency tuning scheme. The results are shown in Fig. 22.

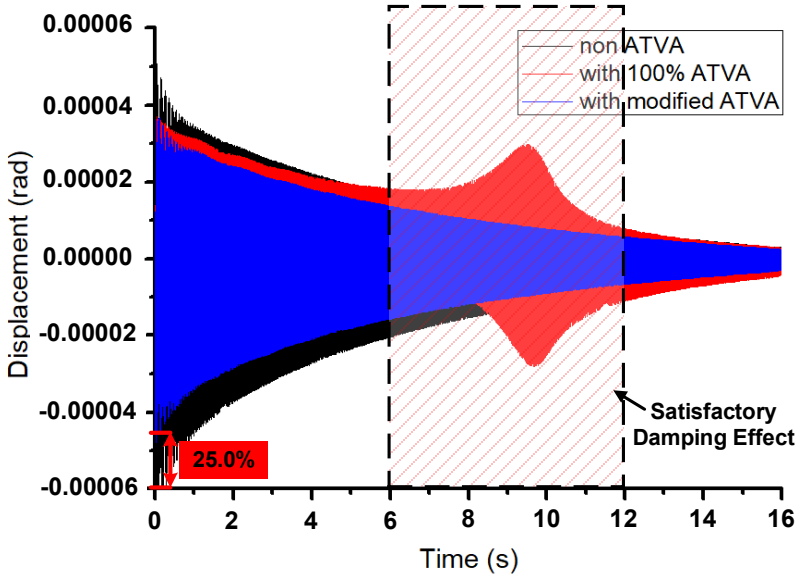


Fig. 22 Comparison of the relative $\theta_3$-$\theta_2$ displacement responses of the three schemes

When the vibration absorber's natural frequency follows the torque excitation 100%, natural vibration coupling appears, and the coupling point enters the resonance area of the excitation frequency, thus degrading the vibration response over a certain time period. The improved frequency tuning scheme can effectively prevent entry of the coupling point into the torque excitation resonance area. The vibration magnitude is reduced by 25.0%. The above result verifies the results of the analysis of the relationship between the dominant external excitation frequency and inherent frequency of the dynamic vibration absorber in Section 4.2.

*5.2 Application of the ATVA on the DCT powertrain in 4$^{th}$ gear*

According to the analysis of the relationship between the torque excitation frequency and system natural frequencies in Section 4.1, when the powertrain works in 4$^{th}$ gear, the 6$^{th}$ natural frequency, 522.6 Hz, passes through the torque excitation frequency range (420-680 Hz), forming resonance point 5. According to the sensitivity analysis in Section 2.2, $J_4$ has a significant impact on the 6$^{th}$ natural vibration. Therefore, the ATVA should be installed near $J_4$. However, $J_4$ is a synchronizer in the powertrain model, precluding absorber installation at this location. $J_3$ and $J_5$ correspond to gear pairs and the differential in the powertrain, respectively, and the absorber cannot be easily installed on these two inertial points either. According to engineering experience, a satisfactory vibration reduction effect can be attained by installing the absorber near the vibration source. Thus, the ATVA is

installed on the engine inertial point $J_1$. The dynamic model is shown in Fig. 16.

Two ATVA frequency tuning schemes are adopted. One is the 100% frequency following scheme, whereas the other frequency tuning scheme is the improved one described in Section 4.2. The vibration absorber parameters are moving inertia $J_A = J_1/5 = 0.08$ kg·m$^2$ and damping $c_A = 1.23$ N·m·s·rad$^{-1}$; the variable stiffness $k_A$ can be calculated according to the frequency tuning scheme adopted and Eq. (15).

Using the relative displacement of $J_1$ and $J_2$ as reference points a comparison is made among the vibration response without the ATVA, with the ATVA in the 100% frequency following scheme and with the ATVA in the modified frequency tuning scheme. The results are shown in Fig. 23.

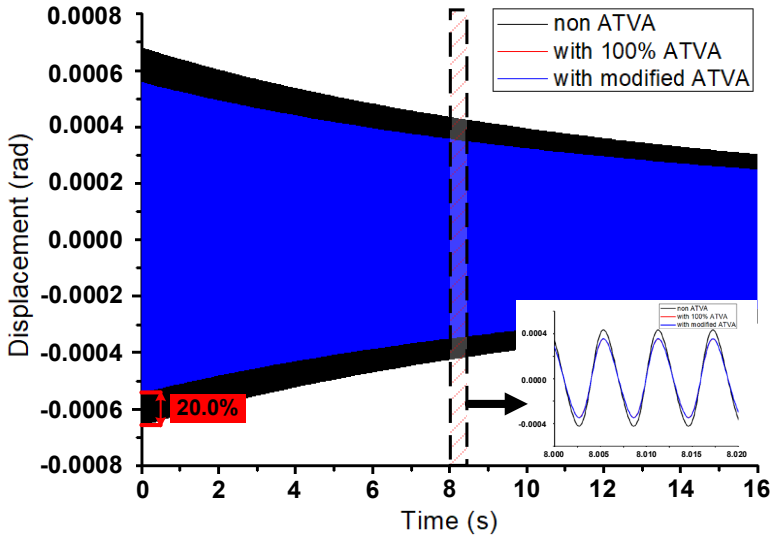


Fig. 23 Comparison of the relative $\theta_2$-$\theta_1$ displacement responses of the three schemes

The vibration magnitude is reduced by 20% by installing the absorber near the vibration source. Relative to the 25.0% vibration magnitude reduction observed in the sensitivity analysis, this result is not optimal but is still notable. There is no vibration deterioration at any time when the 100% following frequency tuning scheme is adopted. The two frequency tuning schemes of the ATVA achieve similar vibration reduction effects. The reason is that the variable natural frequency caused by the ATVA does not couple with any other system natural vibrations, and the variable natural vibrations of the powertrain do not enter the excitation resonance area. This result verifies the necessity of studying the relationship between the torque excitation frequency and absorber natural frequency. In addition, a comparison of the vibration

magnitude reductions in Fig. 22 and in Fig. 23 shows the importance of the ATVA installation position. The ATVA installation position can be obtained by studying the relationship between the torque excitation frequency and system natural frequencies in Section 4.1 and the sensitivity analysis of the eigenvalues of each order for each inertial element in Section 2.2.

From the above analysis, according to the relationship between the torque excitation frequency and system natural frequencies and the sensitivity analysis results, the absorber installation position and stiffness range can be determined. According to the relationship between the torque excitation frequency and absorber natural frequency, if the coupling point of the transient changeable natural vibration frequencies of the powertrain is prevented from entering the torque excitation resonance area, the optimal frequency tuning scheme can be attained. In engineering applications, to ensure that the ATVA can accommodate all working conditions and achieve the optimal vibration reduction effect, we should install an ATVA group on the powertrain in the proper position and perform parameter optimization and coordinate control to achieve a satisfactory vibration response.

## 6. Conclusion

In this paper a dynamic model of the dual lay-shaft format of the DCT powertrain was established, and a natural vibration characteristic analysis of the powertrain system and sensitivity analysis of the eigenvalues of each order for each inertial point were performed. A detailed engine model and vehicle resistance model were integrated into the dynamic model, improving the boundary conditions of the dynamic model.

Based on the dynamic model, the main factors affecting the torque excitation dominant frequency were studied, such as the transient gear shifting process, engine speed and gear ratios. Gear shifting is a transient process with a short duration and thus has little influence on the dominant frequency of torque excitation. The ATVA can only follow the dominant frequency and cannot accurately follow the gear shifting process. Therefore, the transient gear shifting process is outside the effective application scope of the ATVA. The external torque frequency increases linearly with engine speed, and the start point and end point increase with gear upshifting. The engine speed and gears are the key factors affecting the torque excitation frequency.

The overall relationships among the system natural frequencies, dominant external excitation frequency and inherent frequency of the ATVA were analysed. Based on the relationship between the dominant external excitation frequency and system natural frequency and the system sensitivity analysis, the absorber installation position and stiffness range were determined. According to the relationship between the excitation frequency and absorber natural frequency, the optimal absorber frequency tuning scheme was designed. Based on our analysis, the ATVA was applied on the DCT powertrain in $2^{nd}$ gear and $4^{th}$ gear with continuously changing engine speed. The simulation results verified the effectiveness and reliability of the ATVA installation position, the stiffness range and the optimal frequency tuning scheme proposed based on the analysis results in this research.

**Acknowledgements**

This work was supported by the National Natural Science Foundation of China (Grant No. 51775040) and the China Scholarship Council (Grant No. 201706030028).

**References**

1 M. Goetz, M.C. Levesley, D.A. Crolla, Dynamics and control of gearshifts on twin-clutch transmissions, Proc. Inst. Mech. Eng. Part D J. Automob. Eng. 219 (2005) 951–963. doi:10.1243/095440705X34720.

2 P.D. Walker, N. Zhang, R. Tamba, Control of gear shifts in dual clutch transmission powertrains, Mech. Syst. Signal Process. 25 (2011) 1923–1936. doi:10.1016/j.ymssp.2010.08.018.

3 Y. Liu, D. Qin, H. Jiang, Y. Zhang, A Systematic Model for Dynamics and Control of Dual Clutch Transmissions, J. Mech. Des. 131 (2009) 061012. doi:10.1115/1.3125883.

4 M. Kulkarni, T. Shim, Y. Zhang, Shift dynamics and control of dual-clutch transmissions, Mech. Mach. Theory. 42 (2007) 168–182. doi:10.1016/j.mechmachtheory.2006.03.002.

5 A.R. Crowther: PhD thesis, Transient vibration in powertrain systems with automatic transmissions, University of Technology Sydney, AUS (2004).

6 N. Zhang, A. Crowther, D.K. Liu, J. Jeyakumaran, A finite element method for the dynamic analysis of automatic transmission gear shifting with a

four-degree-of-freedom planetary gearset element, Proc. Inst. Mech. Eng. Part D J. Automob. Eng. 217 (2003) 461 – 474. doi:10.1243/095440703766518096.

7 P. Couderc, J. Callenaere, J. Der Hagopian, G. Ferraris, A. Kassai, Y. Borjesson, L. Verdillon, S. Gaimard, Vehicle driveline dynamic behaviour: Experimentation and simulation, J. Sound Vib. 218 (1998) 133–157. doi:10.1006/jsvi.1998.1808.

8 A.R. Crowther, R. Singh, N. Zhang, C. Chapman, Impulsive response of an automatic transmission system with multiple clearances: Formulation, simulation and experiment, J. Sound Vib. 306 (2007) 444–466. doi:10.1016/j.jsv.2007.05.053.

9 C.L. Gaillard, R. Singh, Dynamic analysis of automotive clutch dampers, Appl. Acoust. 60 (2000) 399–424. doi:10.1016/S0003-682X(00)00005-0.

10 Z.B. Xu: PhD thesis, Study on Adaptive Tuned Vibration Absorbing Technology, University of Science and Technology of China, CHN (2010).

11 D. Zhang: Master Thesis, Optimizing the parameters of dynamic vibration absorber and researching on the active control, Changan University, CHN (2015).

12 K. Williams, G. Chiu, R. Bernhard, Adaptive-passive absorbers using shape-memory alloys, J. Sound Vib. 249 (2003) 835–848. doi:10.1006/jsvi.2000.3496.

13 C.L. Davisa, G.A. Lesieutrea, J. Doschb, C.L. Davis, G.A. Lesieutre, J. Dosch, A tunable electrically shunted piezoceramic vibration absorber, SPIE. 3045 (1997) 51–59.

14 H.X. Deng, X.L. Gong, Adaptive tuned vibration absorber based on magnetorheological elastomer, in: J. Intell. Mater. Syst. Struct., 2007: pp. 1205–1210. doi:10.1177/1045389X07083128.

15 J. Fu, P. Li, G. Liao, J. Lai, M. Yu, Development and Dynamic Characterization of a Mixed Mode Magnetorheological Elastomer Isolator, IEEE Trans. Magn. 53 (2017). doi:10.1109/TMAG.2016.2606406.

16 L.J. Qian, F.L. Xin, X.X. Bai, N.M. Wereley, State observation–based control algorithm for dynamic vibration absorbing systems featuring magnetorheological elastomers: Principle and analysis, J. Intell. Mater. Syst. Struct. 28 (2017) 2539–2556. doi:10.1177/1045389X17692047.

17 K. Lu, L. Liu, Z. Yang, X. Gong, Z. Rao, Z. Xie, Semi-active dynamic absorber of a ship propulsion shafting based on MREs, Zhendong Yu Chongji/Journal Vib. Shock. 36 (2017). doi:10.13465/j.cnki.jvs.2017.15.006.

18 N. Hoang: PhD thesis, An adaptive tunable vibration absorber using magnetorheological elastomers for vibration control of vehicle powertrains, University of Technology Sydney, AUS (2011).

19 P. Gao, C. Xiang, H. Liu, H. Zhou, Reducing variable frequency vibrations in a powertrain system with an adaptive tuned vibration absorber group, J. Sound Vib. 425 (2018) 82–101. doi: 10.1016/j.jsv.2018.03.034.

20 P.D. Walker, N. Zhang, Transmission of Engine Harmonics to Synchronizer Mechanisms in Dual Clutch Transmissions, J. Vib. Acoust. Asme. 136 (2014). doi:Artn 05100910.1115/1.4028079.

21 X.D. Su: PhD thesis, Study on Brake Vibration and Noise Reduction Methods using Substructure Sensitivity Analysis and Structural Modification Techniques, Tsinghua University, CHN (2003).

22 Z.F. Fu, H.X. Hua, Modal Analysis Theory and Application, Shanghai Jiao Tong University Press, Shanghai, 2000.

23 P. Gao, Y.H. Wu. Effect of Brake Pressure on High Frequency Braking Squeal of Disc Brakes, J. Northeast. Univ. 38 (2017) 1303-1308.

24 P.D. Walker, N. Zhang, Parameter study of synchroniser mechanisms applied to dual clutch transmissions[J]. Int. J. Powert. 1 (2011) 198-220.

25 C.F. Taylor, The Internal-combustion Engine in Theory and Practice: Combustion, fuels, materials, design. MIT press, Massachusetts, 1985.

26 P.D. Walker, N. Zhang, W. Zhan, B. Zhu, Modelling and simulation of gear synchronisation and shifting in dual-clutch transmission equipped powertrains, Proc. Inst. Mech. Eng. Part C J. Mech. Eng. Sci. 227 (2013) 276–287. doi:10.1177/0954406212449550.

27 P. Walker, B. Zhu, N. Zhang, Powertrain dynamics and control of a two speed dual clutch transmission for electric vehicles, Mech. Syst. Signal Process. 85 (2017) 1–15. doi:10.1016/j.ymssp.2016.07.043.

28 M. Awadallah, P. Tawadros, P. Walker, N. Zhang, Dynamic modelling and simulation of a manual transmission based mild hybrid vehicle, Mech. Mach. Theory. 112 (2017) 218–239. doi:10.1016/j.mechmachtheory.2017.02.011.

29 N. Huang, Z. Shen, S. Long, M. Wu, H. SHIH, Q. ZHENG, N. Yen, C. Tung, H. Liu, The empirical mode decomposition and the Hilbert spectrum for nonlinear and non-stationary time series analysis, Proc. R. Soc. A Math. Phys. Eng. Sci. 454 (1998) 995, 903. doi:10.1098/rspa.1998.0193.

30 N.E. Huang, Z. Shen, S.R. Long, A NEW VIEW OF NONLINEAR WATER WAVES: The Hilbert Spectrum, Annu. Rev. Fluid Mech. 31 (1999) 417–457. doi:10.1146/annurev.fluid.31.1.417.

31 P. Flandrin, G. Rilling, P. Goncalves, Empirical mode decomposition as a filter bank, IEEE Signal Process. Lett. 11 (2004) 112–114. doi:10.1109/LSP.2003.821662.

32 J.C. Wachel, F.R. Szenasi, Analysis of torsional vibrations in rotating machinery, Proc. Turbomach. Sym. 22 (1993) 127–151.

**Correspondence address**

Hui Liu

Beijing Institute of Technology

Beijing 100081

Beijing

P.R. China

Tel.: +86-13701074363

E-mail: liuhui_bit@163.com

**Figures Captions**

Fig.1 Schematic diagram of the powertrain

Fig.2 Corresponding modal shapes

Fig.3 Sensitivity of the $1^{st}$ -order eigenvalue

Fig.4 Sensitivity of the $2^{nd}$ -order eigenvalue

Fig.5 Sensitivity of the $3^{rd}$ -order eigenvalue

Fig.6 Sensitivity of the $4^{th}$ -order eigenvalue

Fig.7 Sensitivity of the $5^{th}$ -order eigenvalue

Fig.8 Sensitivity of the $6^{th}$ -order eigenvalue

Fig.9 Instantaneous engine torque as a percent of the mean torque

Fig.10 Clutch pressure signal

**Tables Captions**